Supporting Information

Polydopamine Nanospheres Coated with Bovine Serum Albumin Permit Enhanced Cell Differentiation: Fundamental Mechanism and Practical Application for Protein Coating Formation

*Behafarid Ghalandari[a], Youyi Yu[a,#], Farnaz Ghorbani[b,#], Antony R. Warden[a], Khan Zara Ahmad[a], Xiao Sang[a], Shiyi Huang[a], Yu Zhang[a], Wenqiong Su[a], Adeleh Divsalar[c], Xianting Ding[a]**

[a] State Key Laboratory of Oncogenes and Related Genes, Institute for Personalized Medicine, School of Biomedical Engineering, Shanghai Jiao Tong University, Shanghai 200030, China

[b] Institute of Biomaterials, Department of Material Science and Engineering, University of Erlangen-Nuremberg, Cauerstraße 6, 91058 Erlangen, Germany

[c] Department of Cell and Molecular Sciences, Faculty of Biological Sciences, Kharazmi University, Tehran, Iran

*Corresponding author: Prof. Xianting Ding; Tel: +86-21-62932274; Fax: +86-021-62932302

E-mail: dingxianting@sjtu.edu.cn

# These authors contributed to this work equally

- **PDANS preparation and characterization**

PDANS was synthesized through the spontaneous oxidation of dopamine hydrochloride under alkali media, according to literature.[1] The morphology of the prepared particles was observed with FE-SEM (TESCAN, Czech Republic) at an accelerating voltage of 15 kV. DLS (Malvern, UK) was used to determine the hydrodynamic diameter of the PDANS. Accordingly, the particles were dispersed in ethanol at 25 °C. The charge density of the particles was evaluated with a zeta sizer (Malvern, UK) at neutral pH, 20% humidity, 1 atm pressure, and 25 °C. The chemical characterization of the constructs was determined using Fourier transforms infrared spectrophotometer (FTIR) (Thermo Fisher Scientific, USA) at wavenumber between 400 and 4000 cm^{-1}.

The chemical characteristics of PDANS are indicated in Figure S1A. The peaks at 3000-3400 cm^{-1} indicate intermolecular hydrogen bonds of dopamine hydrochloride. In addition, aromatic O-H asymmetric stretching vibration is observed at peaks 2958, 3033, 3064, and 3145 cm^{-1}. During oxidative polymerization, the NH_2 in dopamine hydrochloride microstructure turned to secondary amine [2], as indicated by the peaks at 2432, 2538, 2638, 2746, and 3211 cm^{-1}, which disappeared after polymerization. Polymerized nanospheres showed a peak of 3200-3500 cm^{-1}, which is related to the stretching vibration of phenolic O-H and N-H bonds in catechol groups.[3] The aromatic ring and N-H peak is observed at 1603 cm^{-1}. The peak at 1511 cm^{-1} is attributed to the N-H stretching vibration of the amide group. The C-O vibration is observed at 1119 cm^{-1}. The peaks at 1344 and 1285 cm^{-1} are assigned to the bending and stretching vibration of phenolic C–O–H.[4]

PDANS form when charges transfer [5] and intra/intermolecular cross-linkings (noncovalent interactions, including hydrophobic interactions [6], hydrogen bonding, and π-π stacking [4]) occur in the dopamine hydrochloride monomer, as indicates in Figure S1B. Oxidation of dopamine hydrochloride in alkali media leads to the formation of dopamine quinone. Then, leucodopaminechrome forms after deprotonation of amine groups, which further initiate the 1,4-Michael addition reaction. Leucodopaminechrome oxidation leads to the formation of dopaminechrome. After re-arrangement, 5,6-dihydroxyindole is created, which then interacts with o-quinone and forms cross-linked PDA.[2,7]

The FE-SEM micrographs and hydrodynamic diameter of the synthesized PDA particles are shown in Figure S1C, exhibiting monodisperse and homogeneous PDANS spheres with smooth

surfaces. Also, uniform spheres are fabricated with a polydispersity index of 0.15. The hydrodynamic average size is ~ 400 nm. The low and narrow polydispersity index demonstrates the synthetization of uni-size and monodisperse PDANS. The surface charge of synthesized PDANS is -31.2 mV in neutral media. The negative surface charge of spheres leads to adequate dispersion in the aqueous media and creates stable suspension. These results are consistent with observations in previous literature.[3]

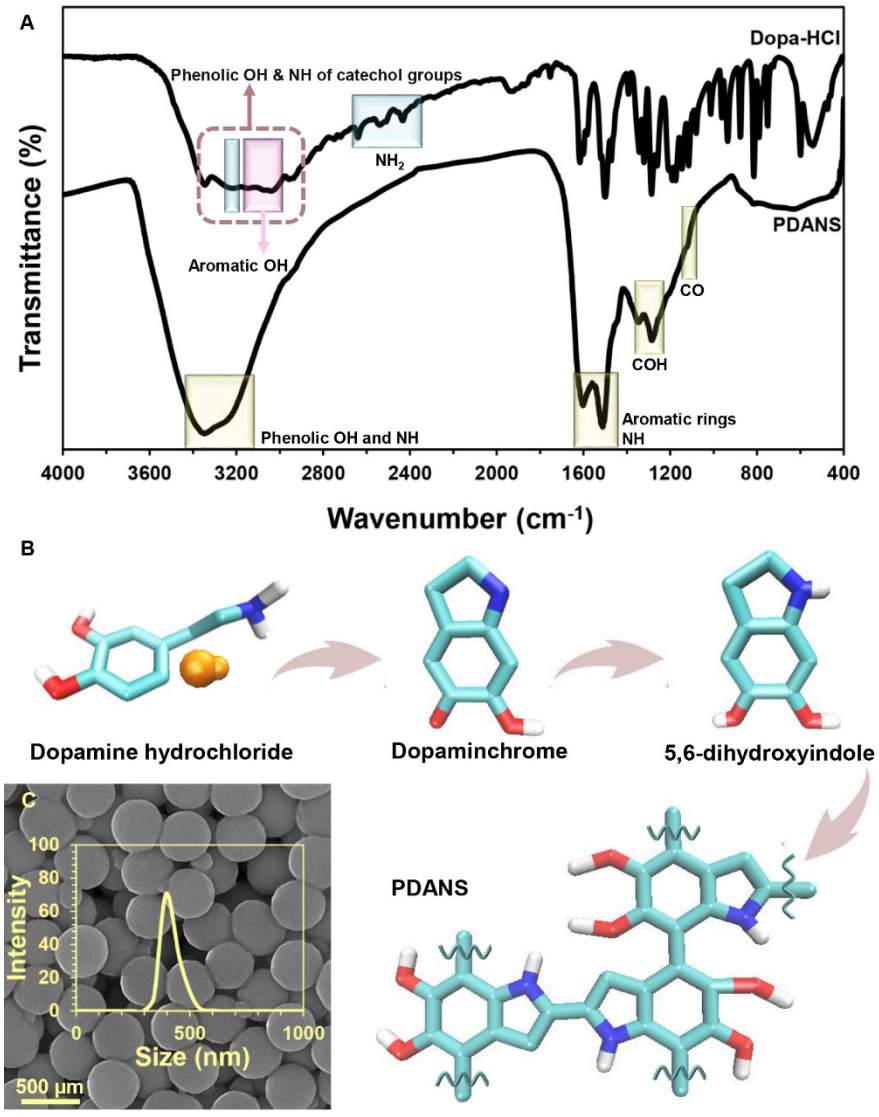

Figure S1: Chemical characterization of PDANS. (A) FTIR spectra of dopamine hydrochloride and PDANS. (B) Schematic of oxidation, re-arrangement, and polymerization of dopamine hydrochloride. (C) FE-SEM micrograph and hydrodynamic size distribution of PDANS.

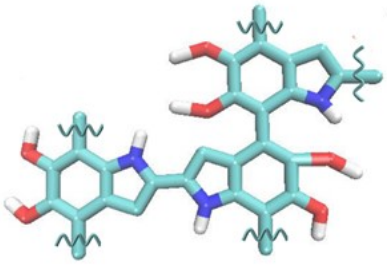

Figure S2: The repeated basic unit of PDANS.

Table S1. The specific sequences of genes for differentiation.

Gene	Length (bp)	Sequence	
		Forward	Reverse
OC	111	CTCACTCTGCTGGCCCTGAC	CACCTTACTGCCCTCCTGCTTG
Col I	234	ACCTCCGGCTCCTGCTCCTCTTAG	GACAGCACTCGCCCTCCCGTTTT
18S	105	GAATTCCCAGTAAGTGCGGGTCATA	CGAGGGCCTCACTAAACCATC

- ***Fluorescence quenching measurements***

The intrinsic fluorescence of BSA is caused by Trp 213, located at the hydrophobic loop in subdomain IIA. As shown in Figure S3A-B, the fluorescence intensity and the maximum intrinsic fluorescence intensity of BSA decreases with the increase of PDANS concentration. The intrinsic fluorescence of BSA is quenched with the increase PDANS concentration. Therefore, PDANS interaction with BSA changes the Trp 213 microenvironment and leads to BSA conformational changes as well. The fluorescence quenching proceeds through diffusive collisions between the fluorophore and the quencher in the excited state (dynamic quenching), the formation of a ground-state complex between the fluorophore and the quencher (static quenching), and simultaneous static and dynamic quenching. The non-linear Stern-Volmer plot suggests a simultaneous static and dynamic quenching mechanism. The Stern-Volmer equation (Equation 1) and the modified Stern-Volmer equation (Equation 2) as follows are applied to perceive the nature of the quenching mechanism.[8].

$$\frac{F_0}{F} = 1 + K_{SV}[Q] = 1 + k_q\tau_0[Q] \quad (1)$$

$$\frac{F_0}{(F_0 - F)} = \frac{1}{f_a K_{SV}} \times \frac{1}{[Q]} + \frac{1}{f_a} \quad (2)$$

where F_0 and F are the fluorescence intensity of BSA in the absence and presence of PDANS, respectively. $[Q]$ is the PDANS concentration. K_{sv} is the Stern-Volmer quenching constant. k_q is the bimolecular quenching rate constant, and τ_0 is the average lifetime of Trp 213 excited state in the absence of quencher (τ_0 = 5.78×10^{-9} s [9]). f_a is the mole fraction of quencher accessible fluorescence. The modified Stern-Volmer equation results are summarized in Figure S4 and Table S2. According to the modified Stern-Volmer plot, BSA's structure changes in the presence of PDANS as Trp 213 is exposed to the solution and accessible for PDANS. The f_a values indicate conformational changes of BSA in the presence of PDANS with increasing temperature. In addition, the K_{sv} values decrease with the increase in temperature. Therefore, a combined static and dynamic quenching is involved in the quenching mechanism, which is initiated by dynamics quenching then with static quenching. In addition, the k_q values are higher than the maximal dynamic quenching constant (2×10^{10} $M^{-1}s^{-1}$). Hence, our analysis confirms the dominant contribution of the static quenching mechanism in BSA interaction with PDANS.

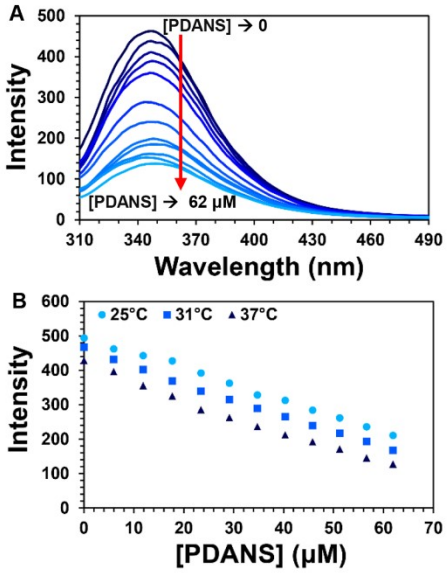

Figure S3: BSA quenching through interaction with PDANS. (A) Fluorescence emission quenching of BSA in the presence of various concentrations of PDANS (0, 6.1, 12, 18, 23.7, 29.2,

35.5, 40, 45.4, 51.3, 55.6, and 62 µM). (B) The maximum fluorescence intensity emission of BSA changes in the presence of the various concentrations of PDANS.

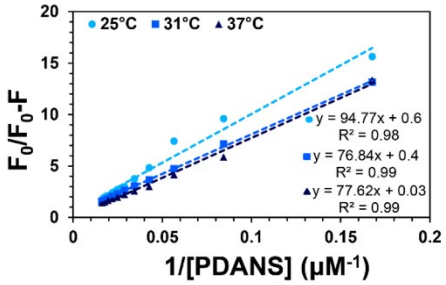

Figure S4: Modified Stern-Volmer plot of BSA quenching through interaction with PDANS.

Table S2. Quenching parameters of BSA's interaction with PDANS.

Temperature (°C)	**f_a**	**K_{sv} ($\times 10^3$ M^{-1})**	**k_q ($M^{-1}s^{-1}$)**
25	1.667	6.33	$1.095\times10^{+12}$
31	2.5	5.21	$9.006\times10^{+11}$
37	3.33	3.86	$6.687\times10^{+11}$

- ***Fluorescence Resonance Energy Transfer (FRET)***

According to the Föster theory, the distance between the donor (here Trp 213) and the acceptor (PDANS) can be calculated with the following equations [10].

$$E = 1 - \frac{F}{F_0} = \frac{R_0^6}{R_0^6 + r_0^6} \quad (3)$$

$$R_0^6 = 8.79 \times 10^{-25} k^2 N^{-4} \Phi J \quad (4)$$

$$J = \frac{\sum F(\lambda)\varepsilon(\lambda)\lambda^4 \Delta\lambda}{\sum F(\lambda)\Delta\lambda} \quad (5)$$

where E is the energy transfer efficiency, R_0 is the critical distance of donor and acceptor where the energy transfer efficiency is 50%, r is the distance between the acceptor and the donor, k^2 is the orientation space factor, N is the refraction index of the medium, Φ is the fluorescence quantum

yield of BSA, and J is the overlap integral of the fluorescence emission spectrum of BSA and the absorption spectrum of PDANS. F(λ) is the correct fluorescence intensity of BSA at the wavelength of λ, and ε(λ) is the molar absorption coefficient of PDANS at the wavelength of λ [11].

The J value is calculated by considering k^2=2/3, N=1.336, and Φ =0.118 [11] in the spectral range of 300-500 nm. The estimated J value is 1.13 $\times 10^{-14}$ cm^3Lmol^{-1}. The values of R_0, r, and E are calculated as 3.17 nm, 3.76 nm, and 0.26, respectively. FRET results confirm the theoretical distance calculation as the obtained value is close to the molecular docking finding between PDANS and Trp 213. The obtained values demonstrate the high probability of Föster energy transfer between BSA and PDANS. Therefore, the static quenching is responsible for BSA fluorescence quenching as FRET evaluation confirms the complex formation between BSA and PDANS.

- ***Binding and thermodynamic parameters evaluations***

According to the quenching mechanism, the binding parameters were calculated using the following equation [12]:

$$\log\left[\frac{F_0 - F}{F}\right] = \log K_a + n\log[Q] \tag{6}$$

where K_a and n are the binding constant and number of binding sites, respectively. The number of binding sites on BSA is close to one for PDANS, and its affinity increases with temperature, demonstrating the endothermic nature of the reaction (Figure S5A and Table S3). To determine the acting forces in the binding site, the entropy changes (ΔS^0) and enthalpy changes (ΔH^0) were calculated with the Van't Hoff equation (Equation 7). The *R* and *T* in the Van't Hoff equation are gas constant and temperature, respectively. The Gibbs free energy change (ΔG^0) was calculated with the following equation (Equation 8) [12].

$$\ln K_a = -\frac{\Delta H^0}{RT} + \frac{\Delta S^0}{R} \tag{7}$$

$$\Delta G^0 = \Delta H^0 - T\Delta S^0 = -RT\ln K \tag{8}$$

The calculated values of ΔS^0 and ΔH^0 are positive (Figure S5B and Table S3), indicating that the interaction of PDANS with BSA is governed by hydrophobic interaction. Also, the negative sign of ΔG^0 (Table S3) revealed the spontaneous binding of PDANS to BSA.

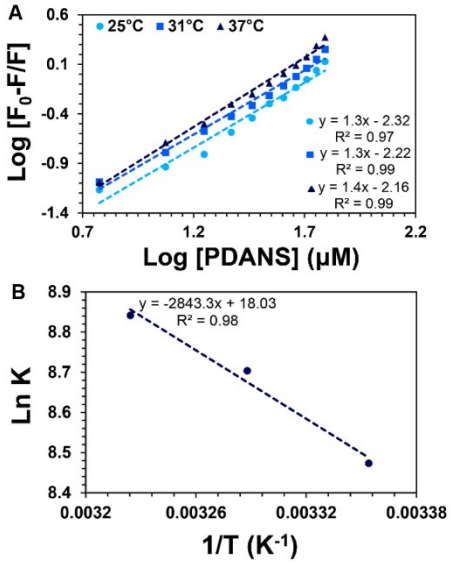

Figure S5: Binding and thermodynamic results of the interaction between BSA with PDANS. (A) Binding logarithmic plot and (B) Van't Hoff plot.

Table S3. Binding and thermodynamic parameters of BSA's interaction with PDANS.

Temperature (°C)	n	K_a ($\times 10^3$ M^{-1})	ΔG^0 (kJ/mol)	$T\Delta S^0$ (kJ/mol. K)	ΔH^0 (kJ/mol)	ΔS^0 (J/mol. K)
25	1.3	4.786	-21.037	44.677		
31	1.3	6.025	-21.936	45.576	23.64	149.85
37	1.4	6.918	-22.835	46.475		

Table S4. Changes in the secondary structure content of BSA in the absence and presence of various concentrations of PDANS at 25 °C.

Concentration (µM)	%α-helix	%β-sheet	%Random coil
0	62.3	17.9	19.8
10	59.6	19.8	20.6
20	58.1	21.2	20.7

30	54.7	23.2	22.1
40	50.3	28.1	21.6
50	48.4	31.1	20.5

Table S5. Surface roughness before and after protein coating treatment.

Sample	Roughness average (S_a)	Root means square roughness (S_q)
PDANS	569 pm	1.27 nm
PDANS coated with BSA	9.72 nm	12.9 nm

- ***BSA interaction with PDANS in the presence of SDS: assessment of quenching mechanism, binding and thermodynamic parameters***

The interaction of BSA with PDANS was evaluated via displacement of the local dielectric environment with 0.5% (w/v) SDS. The fluorescence intensity (Figure S6) and the maximum intrinsic fluorescence intensity (Figure S7A) of BSA are quenched with increasing PDANS concentration. The calculated quenching parameters considering Equations 1 and 2 (Figure S7B and Table S6), indicating a combined static and dynamic quenching is involved in the quenching mechanism, which confirms the dominant contribution of the static quenching mechanism in BSA interaction with PDANS in the presence of 0.5% (w/v) SDS.

As shown in Figure S7C and Table S7 calculated by Equation 6, the PDANS binding sites number on BSA is close to one. Also, its affinity decreases with the temperature, demonstrating the exothermic nature of the reaction. The calculated values of ΔS^0 and ΔH^0 using Equation 7 are negative (Figure S7D and Table S7), indicating the interaction of PDANS with BSA is governed by hydrogen bond and Van der Waals interactions. The negative sign of ΔG^0 (Table S7) calculated with Equation 8 reveals the spontaneous binding of PDANS to BSA in the presence of 0.5% (w/v) SDS.

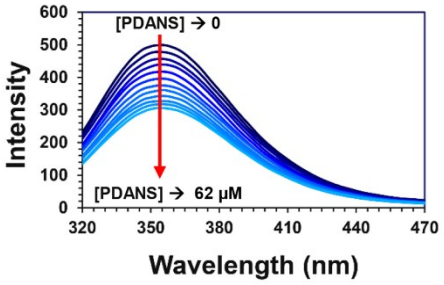

Figure S6: Fluorescence emission quenching of BSA in the presence of various concentrations of PDANS (0, 6.1, 12, 18, 23.7, 29.2, 35.5, 40, 45.4, 51.3, 55.6, and 62 µM) via displacement of the local dielectric environment with 0.5% (w/v) SDS.

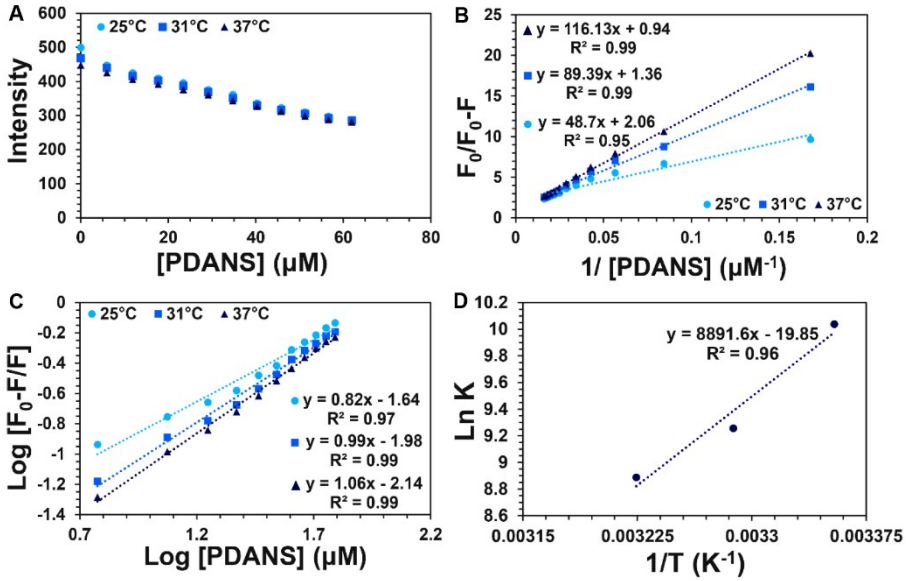

Figure S7: Quenching mechanism, binding, and thermodynamic results of BSA interaction with PDANS via displacement of the local dielectric environment with 0.5% (w/v) SDS. (A) The maximum fluorescence intensity emission of BSA changes in the presence of the various concentrations of PDANS. (B) Modified Stern-Volmer plot of BSA quenching through interaction with PDANS. (C) Binding logarithmic plot. (D) Van't Hoff plot.

Table S6. Quenching parameters of BSA's interaction with PDANS in the presence of 0.5% (w/v) SDS.

Temperature (°C)	**f_a**	**K_{sv} ($\times 10^3$ M^{-1})**	**k_q ($M^{-1}s^{-1}$)**
25	0.49	42.29	$7.32\times10^{+12}$
31	0.74	15.21	$2.63\times10^{+12}$
37	1.06	8.09	$1.4\times10^{+12}$

Table S7. Binding and thermodynamic parameters of BSA's interaction with PDANS in the presence of 0.5% (w/v) SDS.

Temperature (°C)	n	K_a ($\times 10^3$ M^{-1})	ΔG^0 (kJ/mol)	$T\Delta S^0$ (kJ/mol. K)	ΔH^0 (kJ/mol)	ΔS^0 (J/mol. K)
25	0.82	22.91	-24.715	-49.205		
31	0.99	10.47	-23.725	-50.195	-73.92	-165.03
37	1.06	7.24	-22.735	-51.185		

References

1 F. Ghorbani, A. Zamanian, A. Behnamghader and M. D. M. D. Joupari, *Mater. Sci. Eng. C*, 2019, **94**, 729–739.

2 F. Yu, S. Chen, Y. Chen, H. Li, L. Yang, Y. Chen and Y. Yin, *J. Mol. Struct.*, 2010, **982**, 152–161.

3 N. Nishizawa, A. Kawamura, M. Kohri, Y. Nakamura and S. Fujii, *Polymers (Basel).*, 2016, **8**, 62–77.

4 J. Fu, Z. Chen, M. Wang, S. Liu, J. J. Zhang, J. J. Zhang, R. Han and Q. Xu, *Chem. Eng. J.*, 2015, **259**, 53–61.

5 Y. H. Ding, M. Floren and W. Tan, *Biosurface and Biotribology*, 2016, **2**, 121–136.

6 Z. Iqbal, E. P. C. Lai and T. J. Avis, *J. Mater. Chem.*, 2012, **22**, 21608–21613.

7 Q. Wei, F. L. Zhang, J. Li, B. J. Li and C. S. Zhao, *Polym. Chem.*, 2010, **1**, 1430–1433.

8 M. R. Eftink and C. A. Ghiron, *Anal. Biochem.*, 1981, **114**, 199–227.

9 U. Anand, C. Jash and S. Mukherjee, *J. Phys. Chem. B*, 2010, **114**, 15839–15845.

10 S. Ghosh, D. Singharoy and S. C. Bhattacharya, *Spectrochim. Acta Part A Mol. Biomol. Spectrosc.*, 2018, **195**, 7–15.

11 J. Liu, Y. He, D. Liu, Y. He, Z. Tang, H. Lou, Y. Huo and X. Cao, *RSC Adv.*, 2018, **8**, 7280–7286.

12 J. KANG, Y. LIU, M. XIE, S. LI, M. JIANG and Y. WANG, *Biochim. Biophys. Acta - Gen. Subj.*, 2004, **1674**, 205–214.